

Fig. 11. Normalized sideband power (filled symbols, left-hand axis) and corresponding modulation indices  $M$  and  $R$  and sideband asymmetry  $S$  (open symbols, right-hand axis) for different power levels of the 4.596 GHz modulation frequency applied to the VCSEL.

lation powers. Both first-order sidebands become stronger than the carrier at modulation powers  $\geq +5$  dBm. Limitations in modulation efficiency can be attributed to imperfect coupling of the radio-frequency signal into the lasers' TO-46 cans, which is evidenced by  $\approx 40\%$  of the applied 4.6 GHz modulation power being reflected by the VCSEL and its TO-46 can.

Figure 10 reports the measured RIN and frequency noise of the VCSEL when emitting in resonance with the Cs  $D_1$  line. The RIN is measured to be  $1 \times 10^{-11} \text{ Hz}^{-1}$  at 10 Hz and  $5 \times 10^{-15} \text{ Hz}^{-1}$  at 10 kHz Fourier frequencies. The frequency noise of the VCSEL is known to be one of the main limitations to the short-term frequency stability of miniature atomic clocks [14], due to frequency-to-amplitude noise conversion in the atomic vapor that degrades the clock's signal-to-noise ratio [5, 15]. As a second effect, the laser frequency noise also limits the frequency stability achievable for the frequency-stabilized laser, which at longer integration times can result in significant clock instability contributions via the frequency light-shift effect [16], as detailed in the following. The PSD of frequency fluctuations  $S_{\Delta\nu}(f)$  of the free-running VCSEL diode (see Fig. 10) is measured as  $S_{\Delta\nu}(10 \text{ Hz}) = 10^{12} \text{ Hz}^2/\text{Hz}$  with a  $f^{-1}$  slope that is signature of a flicker frequency noise. The PSD of *relative* frequency fluctuations is described in terms of  $S_y(f) = S_{\Delta\nu}/\nu_0^2$  where  $\nu_0$  is the laser frequency ( $3.35 \times 10^{14} \text{ Hz}$ ). Describing the frequency noise spectrum by the power law model  $S_y(f) = \sum_{i=-2}^2 h_i f^i$ , we obtain  $h_{-1} = 10^{13}/\nu_0^2 = 8.9 \times 10^{-17}$ . This yields an expected laser frequency stability (in terms of Allan deviation) of  $\sigma_y(\tau = 1s) = \sqrt{h_{-1} 2 \ln 2} = 1.1 \times 10^{-8}$  [17]. In order to verify this estimation, we measured the relative frequency stability of the VCSEL in the free-running and frequency-stabilized regimes (see Fig. 12) by detecting the frequency beatnote between the VCSEL and a narrow-linewidth distributed feedback (DFB) laser [18].

The laser frequency is stabilized on the position of maximum optical absorption of a cm-scale reference Cs cell by modulating the laser direct current at 60 kHz and demodulating the absorption signal on a photodiode with a lock-in amplifier. The resulting correction signal was applied to the VCSEL current, thus providing sufficiently high servo bandwidth. No radio frequency modulation is applied. In the free-running regime, the short-term frequency stability is measured as  $1 \times 10^{-8}$  at 1 s, in agreement with the frequency noise measurements. For the frequency-stabilized VCSEL the stability is improved to  $8 \times 10^{-9}$  at 1 s and to about  $4 \times 10^{-9}$  at  $10^4$  s integration time. We use this latter result and a frequency-light-shift coefficient of

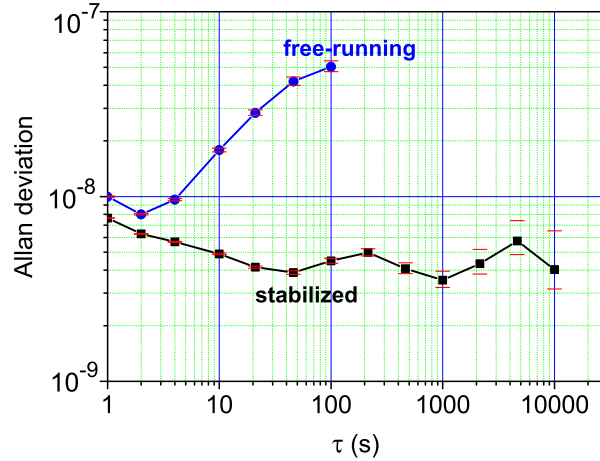


Fig. 12. Allan deviation of the VCSEL frequency, in frequency-stabilized and free-running regimes. The VCSEL is locked to the center of a homogeneously broadened optical Cs absorption line.

$\delta v_{clock}/\delta v_0 = -20$  mHz/MHz reported for VCSEL-driven CPT [19] to estimate the impact on the clock stability. The resulting clock instability contribution from the frequency light-shift is on the level of  $2 \times 10^{-12}$  at  $\tau \approx 10^4$  s, which is compatible with the typical specifications for miniature atomic clocks.

#### 4. CPT clock experiment

Figure 13 shows a simplified scheme of the Cs CPT clock experimental setup. The laser source is a custom-designed grating relief VCSEL resonant at 894.6 nm developed by Ulm University, as described in Section 2.2. It is operated at 1.3 mA and 30°C, to be resonant with the Cs D<sub>1</sub> line. The linewidth of the grating relief VCSEL is measured to be  $\approx 25$  MHz, comparable to those reported in section 3 for the standard VCSELs. The optical output of the laser is collimated into a 2-mm diameter beam and sent through a linear polarizer and a quarter-wave plate. The laser power incident to the Cs cell is about 22  $\mu$ W. The injection current of the laser is directly modulated at 4.596 GHz using a commercial frequency synthesizer and the modulation power was adjusted to  $-2$  dBm for maximum CPT signal height. The Cs microfabricated cell, realized according to the process described in [20], is 2 mm in diameter, 1.4-mm long, and is filled with Ne buffer gas. The cell is temperature-stabilized to  $\approx 80^\circ\text{C}$  where the temperature-dependence of the Cs clock frequency is cancelled [21–23]. A static magnetic field of several  $\mu\text{T}$  is applied to the cell, placed in a single-layer mu-metal magnetic shield. The laser power is detected at the output of the cell with a photodiode that provides signals for two servo loops. The first one serves to stabilize the laser frequency to the center of the homogeneously-broadened optical absorption line; the second one provides the CPT signal and can be used to stabilize the local oscillator (LO) frequency to the center of the CPT resonance for clock operation.

Figure 14 displays the CPT clock resonance signal fitted by a Lorentzian profile. The CPT linewidth is 1.04 kHz at 80°C cell temperature and does not vary significantly in the 70–90°C range (CPT signals with only slightly larger linewidth were observed previously [24] using the standard VCSELs described in section 2.1). The contrast  $C$  (ratio between the signal amplitude  $S$  and the background  $B$ ) is 0.93 %. The corresponding error signal has a discriminator slope  $D$  of typically  $0.9 \times 10^{-6}$  V/Hz. The detection noise  $N$  at the LO modulation frequency is

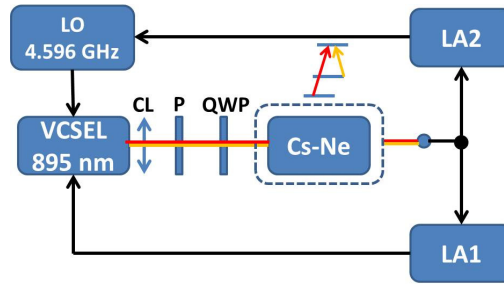


Fig. 13. Cs CPT clock experimental setup. CL: collimation lens; P: polarizer; QWP: quarter-wave plate. LA1 and LA2 are lock-in amplifiers.

$1.7 \times 10^{-7} \text{ V}/\sqrt{\text{Hz}}$ . With  $\nu_C = 4.596 \text{ GHz}$  the expected short-term stability of the clock is then  $\sigma_y(\tau) = \tau^{-1/2} N / (\sqrt{2} \nu_C D) = 2.9 \times 10^{-11} \tau^{-1/2}$  at averaging times  $\tau \approx 1 \text{ s}$  (at  $80^\circ\text{C}$  cell temperature). These results prove that the VCSELs are ideal candidates for the development of high-performance miniature atomic frequency standards based on CPT.

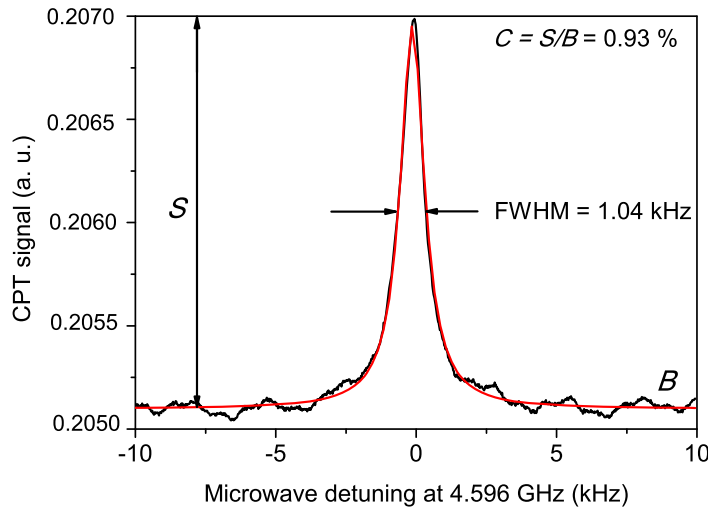


Fig. 14. CPT resonance line in the Cs-Ne microfabricated cell heated to  $80^\circ\text{C}$ . Experimental data are fitted by a Lorentzian profile. The resonance linewidth is 1.04 kHz and the contrast  $C$  is 0.93 %.

## 5. Conclusions

We have studied the spectral properties of custom-designed VCSELs emitting at 894.6 nm, in view of their suitability for the development of miniature atomic clocks based on CPT. VCSELs of two different designs were studied here: grating relief VCSELs featuring improved stability of the emitted light polarization and standard VCSELs without this grating option. Very similar optical linewidths were measured for VCSELs of both design options, in agreement with the measured frequency noise and laser frequency stabilities. Due to the similar linewidths, the frequency noise and frequency stability are concluded to be on comparable levels as well for both VCSEL designs. Analysis of the observed CPT signals shows that the grating relief VCSELs are very well suited for the development of high-performance miniature atomic clocks

based on CPT, in particular because they avoid polarization switches that can be detrimental to the performance of a CPT clock [25]. When combined with previously reported results for standard VCSELs [24], we conclude that both laser designs studied are highly suitable for use in miniature atomic clocks based on CPT on the Cs D1 line.

### **Acknowledgments**

This work was supported by the EC within FP7 (grant no. 224132, MAC-TFC project) and by the Swiss National Science Foundation (SNSF grant no. 200020-140681). C. A. also acknowledges support from the SNSF under sinergia grant no. CRSI20\_122693. The authors thank Philippe Abbé (FEMTO-ST), P. Scherler, and M. Dürrenberger (both UniNe-LTF), for technical support.